High intrinsic activity of CeVO4-based catalysts for ammonia-SCR: Influence of the parameter synthesis

Sylvain Gillot, Jean-Philippe Dacquin, Christophe Dujardin, Pascal Granger

High intrinsic catalytic activity of $CeVO_4$-based catalysts for ammonia-SCR : Influence of the parameter synthesis

S. Gillot, J.P. Dacquin, C. Dujardin*, P. Granger*

Unité de Catalyse et de Chimie du Solide, UMR 8181, Université Lille1 Sciences et Technologies, 59650 – Villeneuve d'Ascq, France

* corresponding authors : email christophe.dujardin@enscl.fr
Tel. +33 …
Fax +33 320 436 561

email pascal.granger@univ-lille1.fr
Tel. +33 320 434 938

Abstract

Promising $CeVO_4$ based materials for the ammonia-SCR catalysts were found as potential substitutes of conventional supported $V_2O_5/WO_3/TiO_2$ catalysts previously optimized for stationary sources. Indeed, the $CeVO_4$ structure can be obtained from hydrothermal synthesis under mild conditions and then stabilized after ageing in wet atmosphere at 600°C. It was found that pH evolutions during hydrothermal synthesis can be an outstanding parameter to get optimal bulk and surface properties since strong acidic medium can be detrimental on the resulting catalytic properties.

Key words : ammonia-SCR, Nitric oxides, Nitrous oxide, vanadium, $CeVO_4$

1. Introduction

Conventional V_2O_5-WO_3/TiO_2 catalysts have been considered in the past two decades as reference to treat off-gases from stationary sources especially NO_x. At moderate temperature ~350°C, the ammonia-Selective Reduction Catalysts leads to a quasi-complete conversion of NO_x with a remarkable selectivity towards nitrogen formation in lean condition (with a large excess of oxygen) [1,2]. Further extrapolation to mobile sources could not be so advantageous because their efficiency is rather limited at low temperature and they currently suffer from significant deactivation at high temperature due to the allotropic transformation of TiO_2 anatase to rutile phase having a much lower specific surface area. Loss of specific surface area can induce significant clustering effects of well-dispersed active VO_x species into larger V_2O_5 aggregates less active and selective to nitrogen production [3]. Hence, these structural modifications could not formally fulfill the standard regulation during the cold start engine and also at high temperatures with related changes in selectivity shifting from ammonia-SCR to ammonia oxidation by oxygen to NO. The subsequent volatilization of vanadium is also a crucial factor in determining the reliability of such end-of-pipe technology due to the high toxicity of vanadium. The stabilization of vanadium in bulk $Ti_{0.9}Ce_{0.05}V_{0.05}O_{2-\delta}$ structure was considered as an important issue attenuating sintering phenomena [4]. However, the development of such materials in previous attempts revealed that the composition of the surface when vanadium is impregnated or mixed with CeO_2 is usually complex with polymeric VO_x and CeO_2 acting as Lewis acid sites whereas $CeVO_4$ would behave like Brønsted acid sites. Hence, these authors suggested that the duality of both V-containing species can explain synergetic effects and can widen the operating window [5]. Promotional effects were also reported on Ce-doped V_2O_5-WO_3/TiO_2 [6] ascribed to the presence of stronger and more active Brønsted acid sites and to a faster reaction between ad-NH_4^+ and NO in the presence of oxygen. Synergetic interactions between Ce, V and W lead to the stabilization of Ce^{3+} species which enhances NO oxidation to NO_2 [6]. We report in this present study the performance of bulk $CeVO_4$ catalysts prepared via a hydrothermal method. It will be shown that changes in the pH conditions during the hydrothermal synthesis may induces significant changes in bulk and surface composition and related catalytic properties especially when the reactional environment becomes strongly acidic.

2. Experimental

2.1. Catalyst preparation and related physicochemical characterization

$CeVO_4$ was synthesized via a hydrothermal route as reported elsewhere [7]. As illustrated in scheme 1, Na_3VO_4 99.98% from Sigma-Aldrich was added to 50 mL of distilled water under vigorous stirring until complete dissolution. An aqueous solution of nitric acid (3M) was further added drops by drops until to reach pH = 1.8. Vanadium-based species were previously found sensitive to change in pH conditions stabilized as $V_{10}O_{28}^{6-}$ or $V_3O_9^{3-}$ oligomeric species [8,9]. In our operating conditions VO^{2+} species would predominate. Once stabilized, $Ce(NO_3)_3.6H_2O$ 99% precursor from Sigma-Aldrich was incorporated and an aqueous solution of sodium hydroxide (1M) was successively added to precipitate cerium and vanadium hydroxides precursors. As reported in Table 1, the sharp drop in pH values at the

end of the hydrothermal treatment can be explained by the following set of Eqs. (1)-(2) leading to the ultimate formation of $CeVO_4$.

$$VO_2^+ + 2HO^- = VO_4^{3-} + 2H^+ \quad (1)$$
$$Ce^{3+} + VO_4^{3-} = CeVO_4 \quad (2)$$

The suspension thus obtained was hydrothermally treated at 180°C for 24 hours.

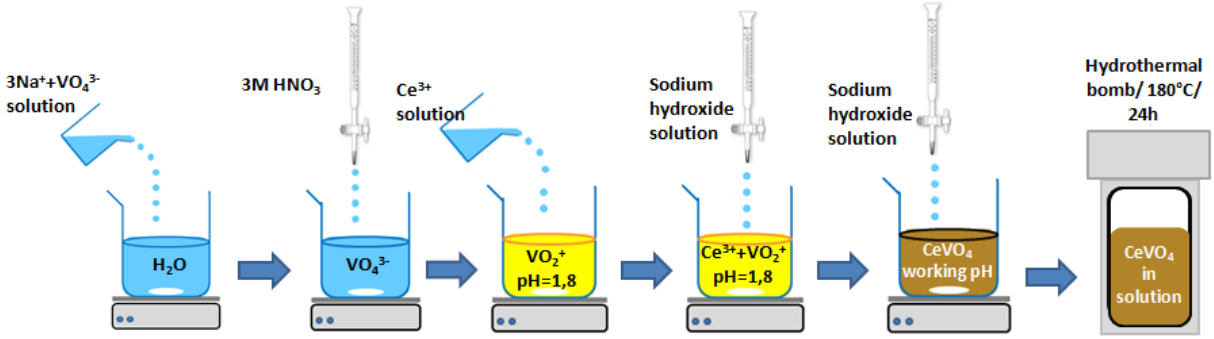

Scheme 1. Steps involved during the hydrothermal synthesis of $CeVO_4$.

$CeVO_4$ was separated by centrifugation, washed abundantly with distilled water and finally with ethanol. As-prepared $CeVO_4$ was dried in air at 80°C for 24h. The solids were aged at 600°C for 5h in a gas mixture composed of air and 10 vol.% H_2O with a time residence of 42.000 $mL.h^{-1}.g^{-1}$. The solid obtained was labelled x-CeV where x stands for the pH values of respectively 2.0, 3.3 and 5.5 measured after hydrothermal synthesis.
Powder X-Ray diffraction (XRD) measurements were carried out at room temperature on a Bruker AXS D8 Advance diffractometer. XPS experiments were performed on an AXIS Ultra DLD Kratos spectrometer equipped with a mono-chromatized aluminium source for excitation (150 W) and charge compensation. The analyzer was operated in a constant pass energy mode (E_{pass} = 40 eV). All binding energies were referenced to the O 1s core level at 530.5 eV. Raman spectroscopic measurements were carried out on a Labram HR Jobin Yvon spectrometer by using an excitation wavelength of 532 nm. H_2 temperature-programmed reduction (H_2-TPR) was performed on a Micromeritics Autochem II 2920 instrument with a flow of 5 vol.% H_2 in Ar and a temperature gradient of 10°C/min. Specific surface area was measured by N_2 physisorption at -196°C with Flowsorb III device.

2.2. Catalytic measurements

Catalytic performances were evaluated on 80 mg weight of catalyst diluted in 1 g SiC in a plug flow reactor from temperature-programmed experiments with a constant heating rate of … °C/min. The global flow rate Q_0 was 333 mL/h insuring a time residence W/Q_0 of 250,000 $mL.h^{-1}.g^{-1}$ with W corresponding to the mass of catalyst. The reaction mixture was composed of 400 ppm NH_3, 400 ppm NO_x, 8 vol.% O_2, 10 vol.% CO_2, 10% H_2O diluted in He with an inlet molar NO/NO_x ratio of 1/2 corresponding to fast-SCR conditions. Online VARIAN CP-4900 μGC analyses led to the quantification of N_2 et N_2O concentration. The outlet gas mixture was analyzed with an infrared IGS Antaris NO_x spectrometer supplied by Thermo Scientific for the quantification of NO, NO_2, NH_3.

3. Results and discussion

3.1. Influence of the pH conditions on the SCR performance of $CeVO_4$.

Overall NO_x conversion profiles and selectivity curves towards N_2O production vs. temperature obtained in fast-SCR conditions (NO/NO_x = 0.5) are collected in Fig. 1. Volcano-type curves are observable which illustrate the usual crucial role of NO_2 as intermediate in the fast-SCR process [10,11]. Generally speaking, the rate determining step corresponds to the re-oxidation of V^{4+}-OH to V^{5+}=O species in vanadia-based catalysts which occurs more readily in the presence of NO_2 rather than oxygen. In fast-SCR conditions more complex parallel and sequential chemical processes can occur with the formation of ammonium nitrites which decompose to nitrogen and ammonium nitrates reduced by NO to ammonium nitrites and then successively converted to N_2. Hence, a complete selectivity can be achieved for optimal NO-to-NO_2 ratio close to 1/1. This explains correctly the different behavior of 3.3-CeV-SCR catalysts, especially $CeVO_4$, at low temperature in fast- and standard-SCR conditions (NO/NO_x = 9/10) according to the following set of reactions :

$2NH_3 + NO + NO_2 = 2N_2 + 3H_2O$ fast-SCR (3)

$2NH_3 + NO + O_2 = 2N_2 + 3H_2O$ standard SCR (4)

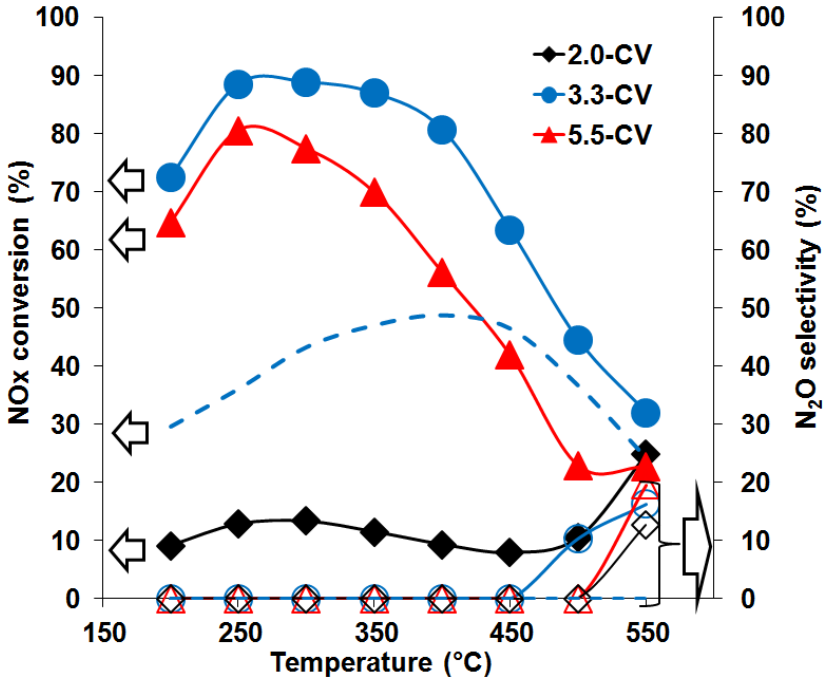

Fig. 1. Influence of pH during the hydrothermal synthesis of the catalytic properties of aged $CeVO_4$ in wet atmosphere at 600°C during the fast- ammonia SCR of NO_x – NOx conversion profile in SCR conditions in dotted line.

As seen, catalytic measurements in standard SCR conditions on 3.3-CeV led to a much lower conversion of approximately 36% vs. 89% at 250°C. On the other the conversion curves converge at high temperature irrespective of the operating conditions.

As observed in Fig. 1, the sharp decrease in NO conversion above 350°C can be partly due to thermodynamic limitations. However, kinetic considerations cannot be ruled out with the involvement of undesirable ammonia oxidation to NO. In addition, side reactions related to the decomposition of ammonium nitrates can partly explain the formation of N_2O in fast-SCR conditions which takes place significantly above 400°C. As seen, significant changes are observable according to pH conditions with optimal catalytic performances on 3.3-CeV corresponding to the highest and broadest conversion profile in the temperature range of the study and ammonia oxidation to NO delayed at high temperature compared to 5.5-CeV. On the other hand, an abnormally low activity in NO_x conversion is observed on 2.0-CeV with

conversion level below 30% in the whole temperature range. Finally, it worthy to note that NO_x are selectively converted to nitrogen, the target molecules, with only a small fraction of N_2O detected only above 450°C reaching a maximum value of 20% at 550°C.

3.2. Bulk vs. surface properties : Tentative correlation with catalytic properties

3.2.1. Bulk properties

XRD patterns recorded on aged $CeVO_4$ samples at 600°C are dominated by the characteristic reflection of the tetragonal $CeVO_4$ phase with the most intense one at $2\theta = 24°$ (see Fig. 1) [12]. Additional X-ray lines appear at $2\theta = 28.5$, 33.2° and 47.7° previously ascribed to the face-centered fluorite structure of CeO_2 except on the sample corresponding to final pH of 2.0 (2,0-CeV) [13]. The characterization of CeO_2 can be explained by the oxidation of Ce^{3+} at ambient temperature according to Eq. (3). On the other hand, the lack of bulk detectable CeO_2 phase in 2.0-CeV is likely due to the highest solubility of $Ce(OH)_3$ in strong acidic medium. Let us note that two weak unknown reflections are discernible at $2\theta = 29.1°$ and 12.2° on 2.0-CeV. As a general trend, those information are in relative good agreement with the slight cerium sub-stoichiometry observed from EDS and fluorescence analysis as indicated in Table 1. The crystallite size of $CeVO_4$ and CeO_2 have been estimated by using the Scherrer equation from the reflections at $2\theta = 24.03$ and …° corresponding to the (200) and (…) planes underlining a greater sensibility of $CeVO_4$ to sintering during thermal aging compared to CeO_2.

$$4Ce(OH)_3 + O_2 = 4CeO_2 + 6H_2O \quad (5)$$

$$Ce(OH)_3 + 3H^+ = Ce^{3+} + 3H_2O \quad (6)$$

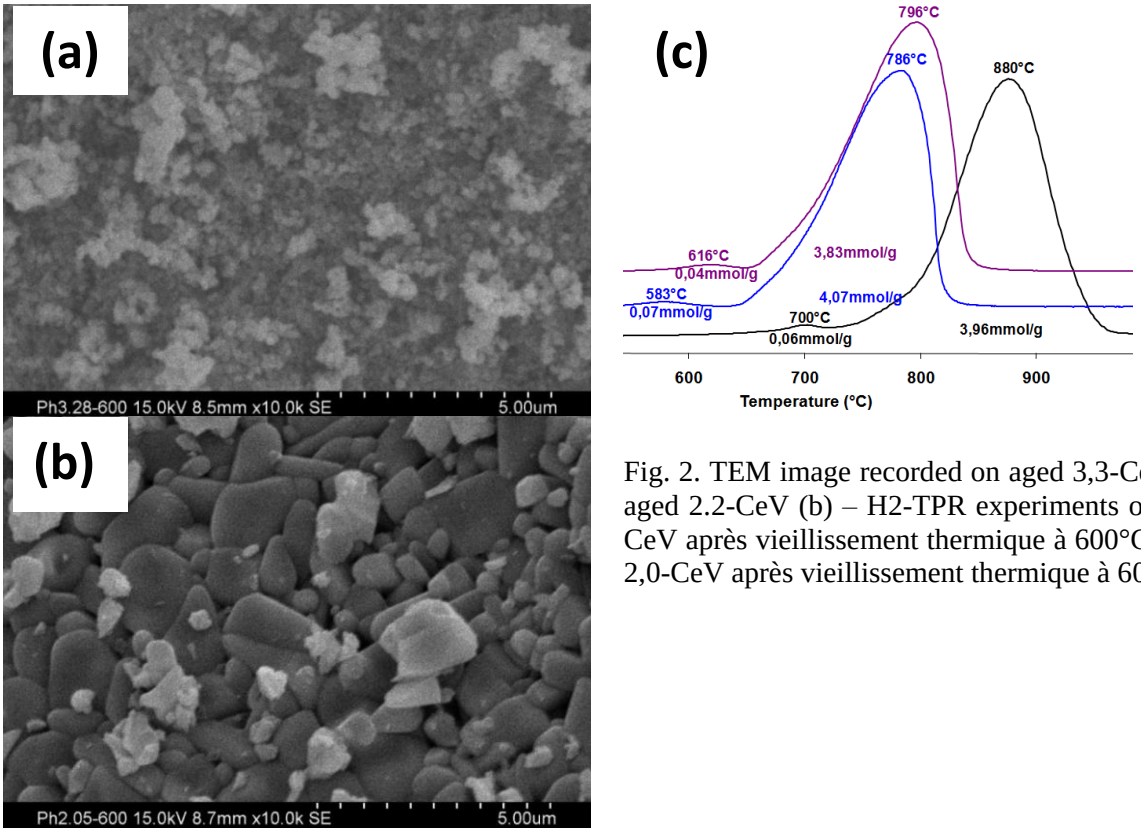

Fig. 2. TEM image recorded on aged 3,3-CeV (a) aged 2.2-CeV (b) – H2-TPR experiments on 3,3-CeV après vieillissement thermique à 600°C – (c) 2,0-CeV après vieillissement thermique à 600°C

A rough comparison of the measured to predicted SSA from XRD data (see S_{th}/S_{exp}) essentially shows that the loss of specific surface area is primarily due to the crystal growth rather than aggregation processes (see Table 1). TEM analysis in Figs. 2(a) and (b) evidences much larger particles on 2.0-CeV with a broader distribution than that observed on 3.3.-CeV. Such modification can be correlated with a significant alteration of reducibility with H_2 consumption profile shifting to much higher temperature on 2.0-CeV.

Raman spectra recorded on $CeVO_4$ samples are collected in Fig. 2 and compared to the characteristic spectral features recorded on reference bulk CeO_2 and V_2O_5 single oxides. A single intense Raman line at 465 cm^{-1} is observed on CeO_2 characterizing the F_{2g} mode of the fluorite phase. Regarding V_2O_5 various Raman lines appear ascribed to V-O-V bridging modes and the terminal V=O bond of vanadia species shifting to high wavenumber at 995 cm^{-1} consistently with the predominance of polymeric vanadyle species [13]. It is worthy to note that these Raman lines ascribed to VO_x species on V_2O_5 oxide are not observed on the spectra obtained on aged $CeVO_4$ samples. The most intense Raman lines at 224, 261, 383, 467, 788, 800 and 862 cm^{-1} are characteristic of $CeVO_4$. Earlier investigations assigned the 862 cm^{-1} Raman lines to A_{1g} vanadate symetric stretching, the 795, 800 cm^{-1} signal to the E_g and B_{2g} antisymetric stretching mode of vanadates and the 368 and 460 cm^{-1} signals to the B_{2g} and B_{1g} deformations [14,15]. The intensity ratio of the Raman signal ascribed to the bridging mode V-O-Ce to the F2g mode ($I_{Ce\text{-}O\text{-}V}/I_{F2g}$) has been calculated. As previously explained the changes observed on the numerical values might reflect the creation of new oxygen vacancies in connection with an increase in Ce^{3+} concentration [13]. Formally, the numerical values thus obtained in Table 2 likely vary within the margin of error revealing no significant influence of pH conditions on the extent of defective sites ascribed to Ce^{3+}.

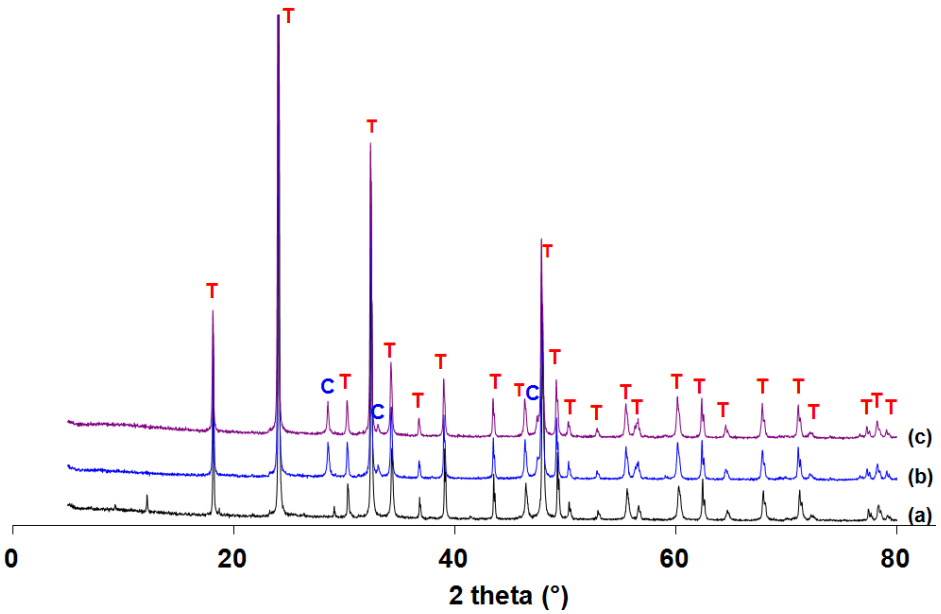

Fig. 3. XRD patterns recorded aged $CeVO_4$ samples at 600°C in a gas mixture composed of air and 10 vol.% H_2O – (T) quadratic phase of $CeVO_4$, (C) cubic structure of CeO_2 – (a) 2.0-CeV; (b) 3.3-CeV; (c) 5.5-CeV

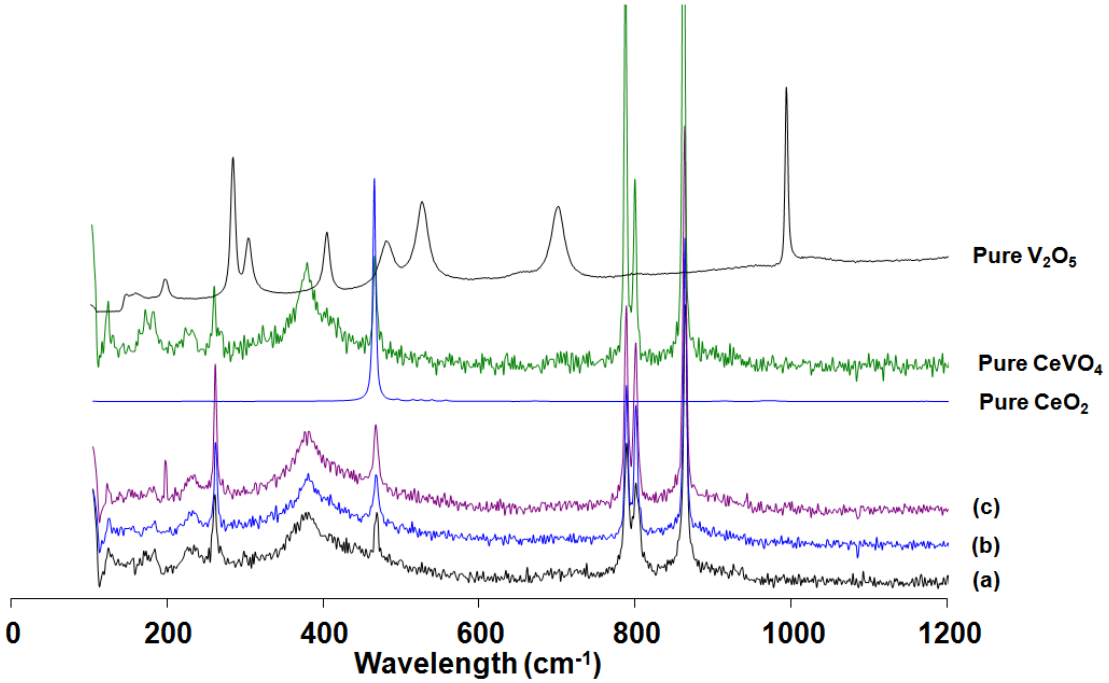

Fig. 2. Raman spectra recorded on aged $CeVO_4$ at 600°C in a gas mixture composed of air and 10 vol.% H_2O. – (a) 2.0-CeV; (b) 3.3-CeV; (c) 5.5-CeV

3.2.2. Surface properties

As exemplified in Table 1, the ageing process induces a sharp decrease in the specific surface area, this trend being more accentuated on aged 2.0-$CeVO_4$ consistently with the TEM and XRD observations with no specific morphology. XPS analysis also reveals changes on the vanadium composition and the oxidation state of cerium oxidic species. The B.E. values for the V $2p_{3/2}$ core level remain quasi-unchanged at 517.7 eV close to the current values ascribed to V^{5+} in V_2O_5 [16]. However the chemical shift on the V $2p_{3/2}$ photopeak for V^{4+} and V^{5+} in composite mixed oxides is rather small being unable to conclude with certainty on the predominance of both species [17]. Previous XPS studies privileged the difference in binding energy between the O1s and V2p3/2 core level to determine the oxidation state of vanadium species [18]. The estimates of ~12.9 eV on all samples are similar to previous values obtained for V^{5+} showing no significant effect on the ageing process [18]. More complex features characterize the Ce 3d core level with two Ce $3d_{5/2}$ and Ce $3d_{3/2}$ photopeaks. Five contributions: u_0, u, u', u'', and u''', and v_0, v, v', v'', and v''', can be extracted from deconvolution as reported elsewhere [19]. The most intense signals, u (v) and u'(v'), reflect in all cases the predominant formation of Ce^{3+}. Quantitative analysis summarized in Table 2 reveals homogeneous V/Ce compositions from the bulk to the surface and confirm through the estimation of the Ce^{4+}/Ce^{3+} ratio the prominent stabilization of Ce^{3+} in agreement with the formation of $CeVO_4$. Prominent information comes from the examination of the Ce^{4+}/Ce^{3+} ratio on aged sample showing an increasing value on Ce^{4+}/Ce^{3+}.

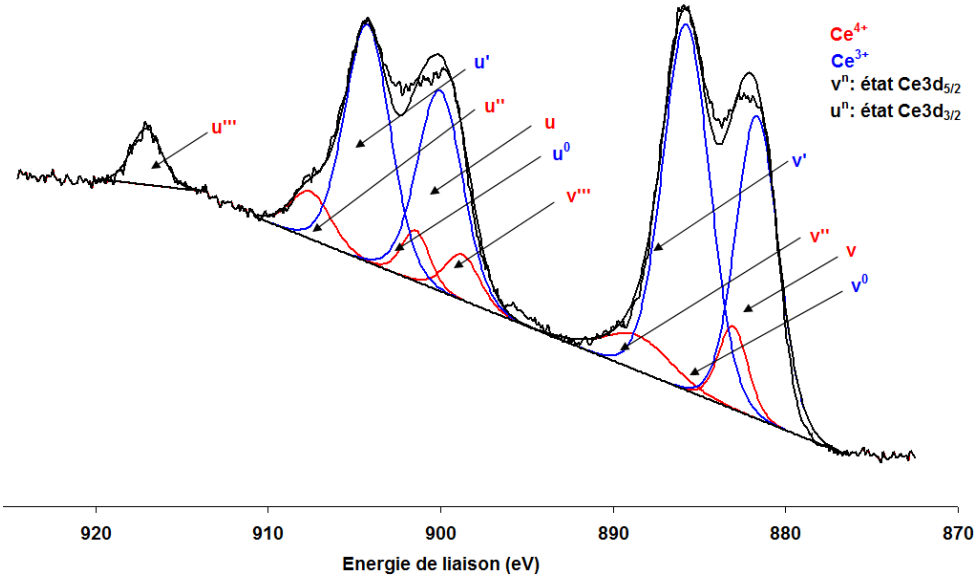

Fig. 3 : Deconvolution on the photopeak charactritic of the Ce 3d core level on $CeVO_4$

The examination of the O 1s photopeak underlines the existence of two different contributions in the range 529.3-530.0 eV and 531.3-531.9 eV assigned to O^{2-} (O_α) from the framework of $CeVO_4$ and chemisorbed oxygen species O^- or O_2^- (O_β) from O_2 adsorption on anionic vacancies [20-22]. As exemplified in Table 2, no significant variation on the O_β/O_α ratio is discernible on as-prepared sample vs. the pH conditions. On the other hand, more significant changes seems to occur on age sample with divergent observations on 2.0-CeV and the two other samples especially 3.3-CeV, for which a decrease in concentration of chemisorbed oxygen species would be related to a lower extent of surface defects. Such a tendency is in rather good agreement with an increase of Ce^{4+}/Ce^{3+} ratio. Based on this observations, the delay observed at high temperature for the preferential catalytic oxidation of ammonia on 3.3-CeV could be partly explained by a lower concentration of active oxygen species.

3.3. General discussion

As found, 2.0-$CeVO_4$ exhibits an abnormally low SCR-activity compared to 3.3- and 5.5-CeV samples despite both samples are characterized by the same structural feature related to the predominance of the quadratic $CeVO_4$ structure. However they differentiate by the absence of bulk detectable CeO_2 phase on 2.0-CeV and change in the textural features since 2.0-CeV (> 1 m^2/g) loses quasi-completely its porosity compared to 3.3- and 5.5-CeV catalysts. As a matter of fact, the lowest specific surface area of 2.0-CeV can partly explain at low temperature the difference observed in NO_x conversion to N_2. Indeed, the decrease in the specific surface area of a factor ~10 seems in relative good agreement with the drops in conversion from 72% on 3.3-VeV to 9% on 2.0-CeV. According, to previous explanations for depicting the behavior of $FeVO_4/TiO_2$-WO_3-SiO_2 [23] in ammonia-SCR, the overall performances of $CeVO_4$ could be partly explained by the alteration of the redox properties due to crystal growth which could explain the low activity of 2.0-CeV. Such an explanation seems consistent with TEM and H_2-TPR observation but is likely invalid at high temperature because all samples converge towards comparable SCR-activity. This suggests that the surface composition and the specific interaction between Ce and vanadium likely contribute. As a matter of fact, the ammonia-SCR performances usually results from complex surface properties combining acidic sites to adsorb ammonia and redox sites to convert NO_x to

nitrogen by reaction with NH_4^+ species. Previous kinetic study of the selective reduction of NO by NH_3 over $V_2O_5(WO_3)/TiO_2$ SCR catalyst led to the identification of the steps and surface species involved in the overall process suggesting that V^{5+}=O as Brønsted acid sites adsorb NH_3 as ammonium ions [24]. Zhang et al. found that the reduced V_2O_5 could promote the formation of superoxide ions (O_2^-) leading to a rate enhancement in NO oxidation to NO_2 vacancies [25].
In the particular case of cerium-vanadium mixed oxides, the composition of the surface when vanadium is impregnated or mixed with CeO_2 is usually complex with polymeric VO_x and CeO_2 acting as Lewis acid sites whereas $CeVO_4$ would behave like Brønsted acid sites […]. Returning to surface analysis from XPS, they revealed the stabilization of V^{5+} species and the coexistence of Ce^{4+} and Ce^{3+} which is consistent with the segregation of CeO_2 and $CeVO_4$ respectively on the most active 3.3-CeV catalyst. XPS data seem consistent with previous statements reporting the stabilization of the pentavalent state of vanadium in $CeVO_4$ [4]. As discussed elsewhere [13], the interaction between ceria and vanadia would stabilize Ce^{3+} sites moderating the valence change Ce^{4+}/Ce^{3+} and blocking the redox behavior of vanadium. Hence, these authors concluded that the redox cycle on ceria-supported vanadia would be preferentially due to cerium sites near vanadium sites. Based on this explanation we can suggest that Ce^{4+}/Ce^{3+} would be involved of oxidation/reduction reaction but we cannot formally rule out the involvement of the V^{5+}/V^{4+} in the overall redox process on $CeVO_4$. Nevertheless, as exemplified in Table 2, the evolution of the Ce^{3+}/Ce^{4+} ratio consistently with O_β/O_α ratio on 3.3-CeV show an good agreement which led to the conclusion the oxidative properties of 3.3-CeV are moderated by a lower concentration of of surface defect compared to 3.3-CeV which probably affect its performances at low temperature especially to oxidize NO to NO. Conversely, a beneficial effect is clearly discernible at high temperature because a lower concentration of active superoxide species delayed the detrimental ammonia axidation to NO.

4. Conclusion

This study was devoted to the catalytic properties of aged $CeVO_4$, prepared by hydrothermal synthesis, once submitted to thermal treatment at 600°C in wet atmosphere. Particular attention was paid to the influence of the pH showing significant structural, textural and surface modification especially when the synthesis was performed in strong acidic medium. The loss of conversion can be rationalized at low temperature essentially by a loss a specific surface area and in the whole temperature conversion to the weaker interaction between cerium and vanadium. It is suggested that the Ce^{4+}/Ce^{3+} play an essential role moderating the surface concentration of anionic vacancies and the active oxygen species for oxidative reaction. This could be detrimental at low temperature for NO oxidation to NO_2 especially under standard conditions. On the other hand, the lowest concentration of defective sites on 3.3-CeV could be beneficial at high temperature slowing down the undesired ammonia oxidation to NO.

Table 1
Physicochemical properties of $CeVO_4$ prepared prepared via hydrothermal method and aged at 600°C

Catalysts	Thermal treatment	Bulk V/Ce[a]	Bulk V/Ce[b]	Crystallite size (nm)		SSA (m^2g^{-1})	SSA (m^2g^{-1})[c]	S_{th}/S_{exp}
				$CeVO_4$	CeO_2	experimental		theoretical
2,0-CeV	As-prepared	1.08	1.3	16.1	-	74.0	78.0	1.1
	Aged[d]			97.9	-	0.5	13	26.0
3.3-CeV	As-prepared	0.94	1.0	26.7	46.0	46.0	47	1.0
	Aged[d]			84.5	56.7	5.8	15	2.6
5.5-CeV	As-prepared	0.95	1.0	13.8	61.9	84.6	91	1.1
	Aged[d]			77.9	73.7	5.4	16	2.9

[a] from X-fluorescence analysis
[b] from EDX analysis
[c] calculated from the average size of $CeVO_4$
[d] after thermal treatment at 600°C for 5 hours air and 10 vol.% H_2O

Table 2
XPS analysis of $CeVO_4$ samples prepared via hydrothermal method and aged at 600°C

Catalyst	Thermal treatment	Bulk V/Ce	B.E. Ce $3d_{5/2}$ (eV)	Ce/O	V/O	V/Ce	Ce^{4+}/Ce^{3+}	O_β/O_α	$I_{Ce\text{-}O\text{-}V}/I_{F2g}$
2,0-CeV	As-prepared	1.09[a]/1.3[b]	883.3	0.29	0.26	0.89	0.12	0.35	1.8
	Aged[c]		883.2	0.22	0.23	1.02	0.12	0.59	2.0
3.3-CeV	As-prepared	0.94[a]/1.0[b]	883.7	0.31	0.24	0.78	0.12	0.34	2.7
	Aged[c]		883.5	0.26	0.25	0.94	0.23	0.27	2.3
5.5-CeV	As-prepared	0.95[a]/1.0[b]	883.6	0.32	0.24	0.77	0.11	0.33	1.6
	Aged[c]		883.3	0.28	0.26	0.91	0.14	0.31	2.4

[a] from X-fluorescence analysis
[b] from EDX analysis
[c] after thermal treatment at 600°C for 5 hours air and 10 vol.% H_2O

Acknowledgments

À compléter

Reference

1. L. Lietti, J.L. Alemany, P. Forzatti, G. Busca, G. Ramis, E. Giamello, F. Bregani, Catal. Today 29 (1996) 143-148.
2. L. Lietti, G. Ramis, F. Berti, G. Toledo, D. Robba, G. Busca, P. Forzatti, Catal. Today 42 (1998) 101-116.
3. G. Madia, M. Elsener, M. Koebel, F. Raimondi, A. Wokaun, Appl. Catal. B 39 (2002) 181-190.
4. B. Guan, H. Lin, L. Zhu, B. Tian, Z. Huang, Chem. Eng. J. 181-182 (2012) 307-322.
5. P.G. Smirniotis, D.A. Peňa, B.S., Angew. Chem. Int. Ed 40(13) (2001) 2479-2482.
6. L. Cheng, J. Li, M. Ge, J. Phys. Chem. C 113 (2009) 21177-21184.
7. B. Xie, G. Lu, Q. Dai, Y. Wang, Y. Guo, Y. Guo, Synthesis of $CeVO_4$ crystals with different sizes and shapes, J. Clust. Sci. 22 (2011) 555-561.
8. R.C. Ropp, B. Caroll, J. Inorg. Nucl. Chem. 39 (1977) 1303.
9. L.D. Sun, Y.X. Zhang, C.H. Yan, C.S. Liao, Y.Q. Lu, Solid State Comm. 124 (2002) 35.
10. E. Tronconi, I. Nova, C. Ciardelli, D. Chatterjee, M. Weibel, J. Catal. 245 (2007) 1-10.
11. I. Nova, C. Ciardelli, E. tronconi, D. Chatterjee, B. Bandl-Konrad Catal. Today 114 (2006) 3-12.
12. R. Cousin, D. Courcot, E. Abi-Aad, S. Capelle, J.P. Amoureux, M. Dourdin, M. Guelton, A. Aboukais, Colloid. Surf. A 158 (1999) 43.
13. H. Huang, Y. Gu, J. Zhao, W. Wang, J. Catal. 326 (2015) 54-68.
14. U. Opara-Krasovec, B. Orel, A. Surca, N. Bukovec, R. Reisfelfd, Solid State Ionics 118 (1999) 195-214.
15. M.V. Martínez-Huerta, J.M. Coronado, M. Fernández-Garcia, A. Inglesias-Juez, G. Deo, J.L.G. Fierro, M.A. Baňares, J. Catal. 225 (2004) 240-248.
16. M. Demeter, M. Neumann, W. Reichelt, Surf. Sci. 454–456 (2000) 41–44.
17. J. Kasperkiewicz, J.A. Kovacich, D. Lichtman, J. Electr. Spect. Relat. Phenom. 32 (1983) 123-132.
18. J. Mendialdua, R. Casanova, Y. Barbaux, J. Electron. Spectrosc. Relat. Phenom. 71 (1995) 249.
19. Romeo, M., Bak, K., El Fallah, J., Lenormand, F., and Hilaire, L., Surf. Int. Anal. 2 (1993) 508.
20. L. Chen, J. Li, M. Ge, J. Phys. Chem. C 113 (2009) 21177-21184.
21. M. Kang, E.D. Park, J.M. Kim, J.E. Yie, Appl. Catal. A 327 (2007) 261.
22. H. Huang, Y. Gu, J. Zhao, X. Wang, J. Catal. 326 (2015) 54-68.
23. G. Wu, J. Li, Z. Fang, L. Lan, R. Wang, T. Lin, M. Gong, Y. Chen, Chem. Eng. J. 271 (2015) 1-13.
24. H. Kamata, K. Takahashi, C.U.I. Odenbrand, J. Catal. 185 (1999) 106-113.
25. S. Zhang, Q. Zhong, W. Zhao, Y. Li, Chem. Eng. J. 253 (2014) 207-216.